# MACHINE LEARNING-BASED INVERSE PROBLEM SOLVING FOR IDENTIFYING HEAT INPUT IN TUNGSTEN INERT GAS (TIG) WELDING

## Z. BOUTALEB, I. BENDAOUD, S. ROUQUETTE, F. SOULIÉ

LMGC, Univ. Montpellier, CNRS, Montpellier, France

**Key words:** GTA welding, heat source modeling, surrogate modeling, parameter estimation,

**Summary.** Thermal cycles occurring during arc welding affect the mechanical properties of the welded parts. Fast heating and cooling cause high thermal gradients which induce plastic flow and, then, residual stresses. Metallurgical changes can also take place according to the material composition. Thermal cycles are a consequence of arc welding heat input. In order predict the thermal field, it is necessary to estimate accurately the thermal loading (heat source). In this work, a methodology is proposed for a fast estimation of heat source parameters based from non-intrusive data (weld pool contour). A surrogate model is established to link the weld pool contour to the heat source parameters. Thus the computational time required for the parameter estimation was significantly reduced in the optimization loop. This methodology is applied to the gas tungsten arc welding process on a thin stainless steel plate with a fully penetrated weld pool. The weld pool was observed on the back side with a camera in order to avoid electrical arc disruption.

## 1 INTRODUCTION

Arc welding is a widely used technique for joining metallic materials. Gas tungsten arc welding (GTAW) is widely used for joining metallic parts in industries such as power plants, petrochemicals, food processing ... Basically, an electric arc is created between a non fusible electrode and the metallic parts to join. The arc produces a local melting of the part edges in contact. A molten pool appears when the metal reaches its melting point. The arc and molten pool are shielded against oxidation with an inert gas. Fluid motions develop within the weld pool and redistribute heat everywhere in the pool. The weld pool grows until heat balance is achieved. Once the welding torch moves away, the liquid metal solidifies, which ensures material continuity.

However, critical defects such as cracking can occur, due to high tensile stresses caused by the local melting (and high local thermal gradients). Structural integrity of welded assemblies is due mainly to the final microstructures in the heat-affected and fuzed zones and the residual stresses [1]. Fast thermal kinetics play a crucial role in final stress states and metallurgical changes in welded components [2]. The thermal field depends on the heat input, so the electrical arc which is directly linked to welding process parameters (current, voltage and welding speed). The prediction of the thermal field with respect to process parameters can be obtained from two approaches: the first consists in a multiphysics modeling of the welding operation (all physical phenomena are taken into account). This approach has the advantage of accurately predicting

heat and mass transfer, weld pool shape ... [3]. Although this approach provides comprehensive physics, it has some limitations. This approach is limited for predicting thermal field of large structures because of computational time. The second approach, the equivalent heat source, reduces the study to a heat conduction problem and, as a consequence, the computational time. Although it does not fully capture the complexity of welding phenomena, it still provides a comprehensive temperature field for most of the structure. The equivalent heat source approach is particularly well suited for predicting the mechanical state of welded components (residual stresses, metallurgical changes ...).

In the literature, several equivalent heat sources have been proposed according to the investigated welding operation. One of the most used equivalent heat source models is the one presented by Goldak [4]. Moreover, other authors have proposed more sophisticated equivalent heat source models that matches more precisely specific welding operations [5, 6]. However, the equivalent heat source approach is defined with several parameters that must estimated.

A classical approach used to estimate unknown parameters is to solve an inverse problem. This approach requires experimental data from intrusive or non-intrusive sensors (temperature, weld pool cross-section ...). Intrusive sensor implementation is not advisable for industrial purposes, especially for wire arc additive manufacturing or multi-pass welding as the thermal sensor must be close to the welded zone to be pertinent.

Kusano et al. [7] studied selective laser melting and deployed a Bayesian optimization approach, which involved finite element calculations for solving inverse problems. They used thermography and cross-sectional bead shapes for the parameter estimation. Hilal [8] developed a digital twinning methodology for calibrating thermal models in the Wire Arc Additive Manufacturing (WAAM) process, focusing on optimizing parameters through Bayesian inverse problem. This approach implements a surrogate model via sparse polynomial chaos expansion and the Markov Chain Monte Carlo (MCMC) adaptive metropolis-Hastings algorithm to estimate the a posteriori probability distributions of unknown modeling parameters on the basis of thermocouple probe thermal measurements. Moselmi et al. [9] compared linear and quadratic regression models, as well as neural networks, for predicting heat source parameters during welding. They used experimental data from thermocouples and molten pool geometry to directly predict unknown modeling parameters.

In this work, a different approach is proposed. The use of finite element calculations is substituted with a surrogate model at each optimization iteration. A surrogate machine learning regression model is used. Additionally, a camera is used to observe non-intrusively and non-destructively the weld pool shape. This non-intrusive technique preserves the integrity of the welding process. By using this non-intrusive technique, the applicability of this methodology can be extended to various welding processes. In summary, the proposed methodology presents an efficient way for the thermal modeling of welding processes and the estimation of heat source parameters. The integration of non-intrusive experimental data and the machine learning approach significantly reduced the computational time of the inverse problem.

## 2  METHODOLOGY

The objective is to estimate heat source modeling parameters by employing non-intrusive and non-destructive camera for recording the weld pool. Experimental arc welding was conducted on a thin stainless steel plate measuring 150 $mm$ in length, 70 $mm$ in width, and 1.5 $mm$ in

thickness. A GTAW welding torch with a tungsten electrode having a diameter of 2.4 $mm$ and sharpened angle of 30° was used to generate a fully penetrated weld pool. In steady state, process parameters are kept constant at 8.58 $V$ for voltage, 81.7 $A$ for current and 2.3 $mm/s$ for the travel speed. The weld pool was shielded against oxidation via the use of argon gas. The camera is positioned on the opposite side to the welding torch in order to observe the fully penetrated weld pool. To enhance the image quality, the plate back side is illuminated with a laser, allowing to distinguish of liquid and solid regions as shown in Figure 1a. An image processing algorithm is used to identify the contour of the weld pool. The weld pool contour is described with rays regularly spaced at an angle of 5° from the weld pool centroïd as illustrated in Figure 1b. The experimental data used as descriptors for the rest of the study are the lengths of these rays.
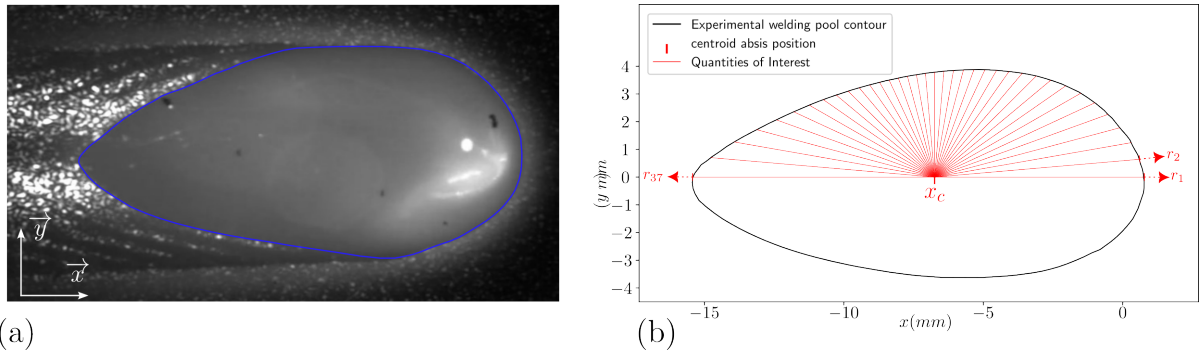


(a) (b)

**Figure 1**: (a) Image of the weld pool on the back side of the plate with contour line traced in dark blue (b) geometry contour description with ray technique.

An overview of the estimation methodology is given in Figure 2. The physical problem is modeled considering a purely conductive assumption with an equivalent heat source (thermal loading). The first step is to create a training database based on a design of experiments covering the range of variation of the main parameters to estimate. For each case, in the design of the experiment, a parametric finite element analysis (FEA) is conducted. From each numerical case, the calculated weld pool is extracted and described with ray lengths similar to those of the method employed for describing the experimental weld pool. The numerical dataset is then used to train a surrogate model linking heat source parameters and weld pool geometry. The estimation of the unknown parameters is achieved with an optimization approach based on the minimization of a cost function. The cost function is defined as the difference between the experimental contour and the predicted contour (or their ray differences at a given angle).
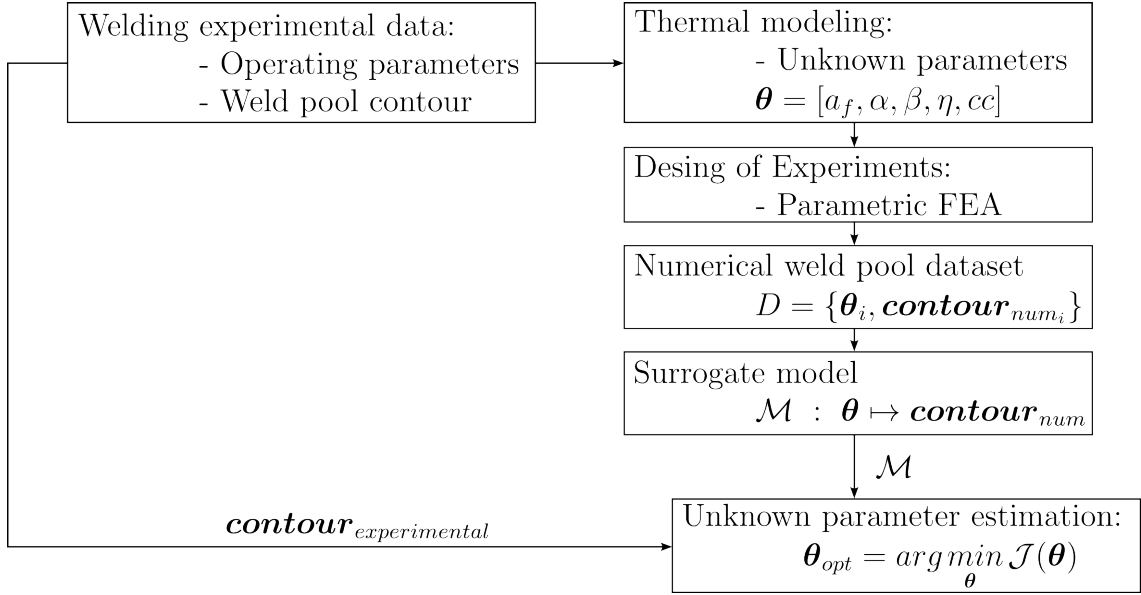
```
┌─────────────────────────────┐        ┌─────────────────────────────────┐
│ Welding experimental data:  │──────▶ │ Thermal modeling:               │
│    - Operating parameters   │        │    - Unknown parameters         │
│    - Weld pool contour       │        │    θ = [a_f, α, β, η, cc]        │
└─────────────────────────────┘        └─────────────────────────────────┘
                                                      │
                                        ┌─────────────────────────────────┐
                                        │ Desing of Experiments:          │
                                        │    - Parametric FEA             │
                                        └─────────────────────────────────┘
                                                      │
                                        ┌─────────────────────────────────┐
                                        │ Numerical weld pool dataset     │
                                        │    D = {θ_i, contour_{num_i}}    │
                                        └─────────────────────────────────┘
                                                      │
                                        ┌─────────────────────────────────┐
                                        │ Surrogate model                 │
                                        │    M : θ ↦ contour_num           │
                                        └─────────────────────────────────┘
                                                      │ M
                                        ┌─────────────────────────────────┐
               contour_experimental    │ Unknown parameter estimation:   │
          ──────────────────────────▶  │    θ_opt = arg min J(θ)          │
                                        │                θ                │
                                        └─────────────────────────────────┘
```

**Figure 2**: Methodology of heat source estimation with a surrogate model linking the weld pool contour to heat source parameters.

## 2.1 THERMAL MODELING

Due to the symmetrical configuration of the experiment, the thermal problem is limited to half of the 316L metal sheet plate as presented in Figure 3.
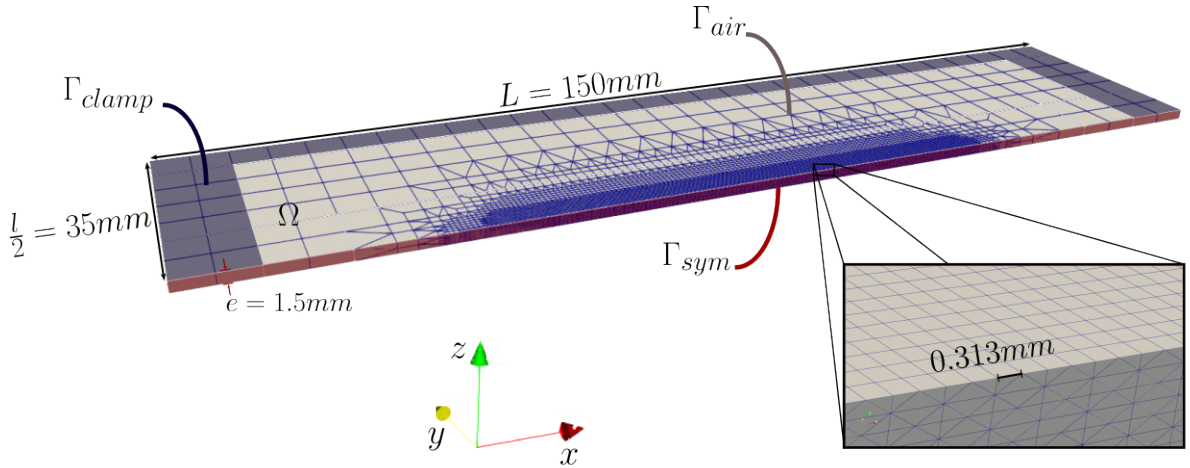


**Figure 3**: Configuration for the Finite Element Analysis: geometry and boundary conditions. The darker zone corresponds to the clamped one.

As underlined previously, a purely conductive modeling is considered and a specific thermal conductivity for the liquid $cc$, in the weld pool, is chosen to take into account the heat transfer due to liquid movements. The thermophysical properties of 316L stainless steel alloys are temperature dependent.

An enthalpic formulation is used for energy conservation, and the equation is written as follows:

$$\frac{\partial H}{\partial t} - \text{div}\left(\lambda(T)\nabla T\right) = 0 \quad \forall(x, y, z) \in \Omega \quad \forall t \in [0, t_f] \tag{1}$$

with the enthalpy $H(T) = \int_{T_0}^{T} \rho C_p(u)\, du$ is interpreted as the heat energy of the material at a given temperature, $\rho$ is the mass density, $C_p$ is the specific heat and $\lambda(T)$ is the thermal conductivity.

Considering the symmetry of the system, on the symmetry surface ($\Gamma_{sym}$), we assume adiabatic heat exchange, described by the following equation:

$$\lambda(T)\frac{\partial T}{\partial n} = 0 \quad \forall(x, y, z) \in \Gamma_{\text{sym}} \quad \forall t \in [0, t_f] \tag{2}$$

For surfaces exposed to air ($\Gamma_{air}$), heat losses due to convection and radiation are considered, as described by the following boundary condition equation:

$$-\lambda(T)\frac{\partial T}{\partial n} = h_{conv}(T - T_\infty) + \epsilon\sigma(T^4 - T_\infty^4) \quad \forall(x, y, z) \in \Gamma_{\text{air}} \quad \forall t \in [0, t_f] \tag{3}$$

For the surfaces in contact with the clamping system ($\Gamma_{clamp}$), the thermal contact is modelled as a convective boundary condition, with higher convective coefficient than the air one, by the following equation:

$$-\lambda(T)\frac{\partial T}{\partial n} = h_{clamp}(T - T_{clamp}) \quad \forall(x, y, z) \in \Gamma_{\text{clamp}} \quad \forall t \in [0, t_f] \tag{4}$$
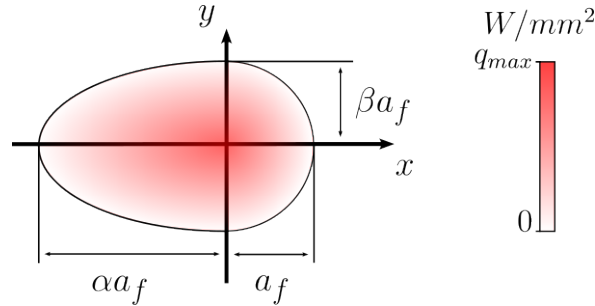


**Figure 4**: Equivalent heat source description.

The moving arc heat input (represented in the Figure 4) is modeled as a double elliptical surface distribution of energy, formulated as follows:

$$
\begin{aligned}
q_f(x, y, t) &= \frac{12\eta UI}{\pi\beta a_f^2(1+\alpha)} \exp\left(-3\left(\left(\frac{(x-vt)^2}{af}\right)^2 + \left(\frac{y}{\beta a_f}\right)^2\right)\right) \quad \forall x \geq 0 \\
q_r(x, y, t) &= \frac{12\eta UI}{\pi\beta a_f^2(1+\alpha)} \exp\left(-3\left(\left(\frac{(x-vt)^2}{\alpha af}\right)^2 + \left(\frac{y}{\beta a_f}\right)^2\right)\right) \quad \forall x < 0
\end{aligned}
\tag{5}
$$

$q_f$ is the front heat source function distribution, and $q_r$ is the rear function distribution. and $\eta$ is the efficiency. This mathematical description takes into account the welding process parameters such as voltage $U$, current $I$, and welding speed $v$ and the process efficiency $\eta$. The origin of the equivalent heat source travels from $x = 45mm$ in the longitudinal coordinate system to the final position at the longitudinal coordinate system $x = 105mm$. The quintuplet $(a_f, \alpha, \beta, \eta, cc)$ is the set of unknown parameters to estimate.

## 2.2 TRAINING DATASET

As an essential step in training the surrogate model, a numerical dataset is generated considering parametric finite element analysis. The design of experiments is created on the basis of Sobol quasirandom sampling; with this sampling method, 128 equally distributed numerical cases are created in the parametric space of the quintuplet: Each unique case of the design of experiments is used as input to perform parametric FEA.

$$\{(a_f, \alpha, \beta, \eta, cc) \in \mathbb{R}^5 : a_f \in [2mm, 5mm]\ \alpha \in [1, 5]\ \beta \in [0.5, 2]\ \eta \in [0.5, 0.8]\ cc \in [1, 5]\} \quad (6)$$
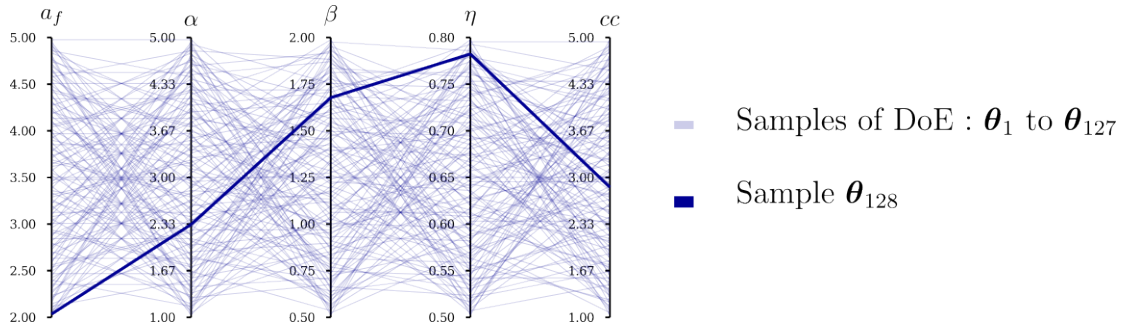


**Figure 5**: Parametric space of quintuplet used for the design of experiments: Each of the 128 cases corresponds to a set of quintuplets $\boldsymbol{\theta}$ defined with a solid line.

A total of 128 FEA are generated within the parametric space. Each numerical case in the design of experiments is a unique combination of heat source parameters (as illustrated in Figure 5). Each of the 128 unique quintuplets is used as input in the parametric FEA. Code aster software is used to solve each FEA case. The meshgrid used considers finer elements in the weld zone (see Figure 3) leading to 19645 nodes, 52725 edge elements, and 40654 volume elements. The average computational time for one FEA simulation is approximately 13 minutes.

Once the parametric FEA calculations are achieved, transient thermal fields are post-processed to extract quantities of interest (QoIs) that is to say: the rays that describe the numerical weld pool (the same technique used to describe the experimental weld pool). In some parametric calculations, the weld pool did not fully penetrated or did not produce a weld pool; therefore, the number of fully penetrated numerical weld pools was 109. The resulting numerical dataset $\mathcal{D} = \{(\boldsymbol{\theta}_i, \boldsymbol{contour}_{num_i}) \mid i \in \{1, 2, 3..., 128\} \setminus \{2, 9, 13, 21, 22, 27, 29, 37, 45, 53, 58, 65, 74, 85, 93, 107, 109, 121, 125\}\}$ consists of 109 pairs of instances and labels (heat modeling parameters — resulting numerical weld pool). To illustrate this dataset, we present a truncated table, due to a lack of space, of some instances and labels in Tables 1 and 2.

6

| | $a_f(mm)$ | $\alpha$ | $\beta$ | $\eta$ | $cc$ |
|---|---|---|---|---|---|
| $\boldsymbol{\theta}_1$ | 3.5 | 3.0 | 1.2 | 0.65 | 3.0 |
| $\boldsymbol{\theta}_3$ | 2.8 | 4.0 | 0.9 | 0.72 | 2.0 |
| $\cdots$ | $\cdots$ | $\cdots$ | $\cdots$ | $\cdots$ | $\cdots$ |
| $\boldsymbol{\theta}_{128}$ | 2.0 | 2.3 | 1.7 | 0.78 | 2.9 |

| | $r_1$ | $r_2$ | $\cdots$ | $r_{37}$ |
|---|---|---|---|---|
| $contour_{num_1}$ | 4.8 | 4.7 | $\cdots$ | 5.1 |
| $contour_{num_3}$ | 6.9 | 6.8 | $\cdots$ | 7.3 |
| $\cdots$ | $\cdots$ | $\cdots$ | $\cdots$ | $\cdots$ |
| $contour_{num_{128}}$ | 6.1 | 6.1 | $\cdots$ | 6.7 |

**Table 1**: (a) Examples of some quintuplets used for the parametric study.

**Table 2**: (b) Numerical contours represented as rays, resulting from the parametric study.

## 2.3 SURROGATE MODEL

The surrogate model is defined as a function $\mathcal{M}$ that maps heat source parameters $\boldsymbol{\theta}$ to the numerical weld pool rays $\boldsymbol{contour}_{\text{predicted}}$ as presented below.

$$\mathcal{M} : \quad \mathbb{R}^5 \quad \rightarrow \quad \mathbb{R}^{37}$$

$$\boldsymbol{\theta} = \begin{bmatrix} a_f \\ \alpha \\ \beta \\ \eta \\ cc \end{bmatrix} \quad \mapsto \quad \mathcal{M}(\boldsymbol{\theta}) = \begin{bmatrix} h_1(\boldsymbol{\theta}) \\ h_2(\boldsymbol{\theta}) \\ \vdots \\ h_{37}(\boldsymbol{\theta}) \end{bmatrix} = \begin{bmatrix} r_1 \\ r_2 \\ \vdots \\ r_{37} \end{bmatrix} = \boldsymbol{contour}_{\text{predicted}}$$

Each ray $r_i$ is independently predicted from other rays via the multivariate polynomial model $h_i$. Polynomial model is a generalization of the linear regression model to largest basis of functions, known as basis function expansion. Note that the surrogate model is linear with weights $\mathbf{w}$ as shown in equation 8. Let's remark that the variable $X_i$ refers to one of the quintuplet $(a_f, \alpha, \beta, \eta, cc)$.

$$h(\mathbf{X}) = w_0 + \mathbf{w}^T \boldsymbol{\phi}(\mathbf{X}) + \epsilon = r \tag{7}$$

Where $\boldsymbol{\phi}(\mathbf{X})$ transformed feature vector.

For example, multivariate polynomial model of second order is written as follow :

$$h(\mathbf{X}) = w_0 + w_1 X_1 + ... + w_n X_n + w_{11} X_1^2 + ... + w_{nn} X_n^2 + w_{12} X_1 X_2 + ... + w_{n-1n} X_{n-1} X_n + \epsilon = y \tag{8}$$

Here the transformed feature vector is :

$$\boldsymbol{\phi}(\mathbf{X}) = (X_1, X_2, ..., X_n, X_1^2, X_2^2, ..., X_n^2, X_1 X_2, X_1 X_3, ..., X_{n-1} X_n) \tag{9}$$

And $w_1, w_2, ..., w_n$ are the coefficients of the linear terms, $w_{11}, w_{22}, ..., w_{nn}$ are the coefficients of the quadratic terms, $w_{12}, w_{13}, ..., w_{1n}, ..., w_{n-1n}$, are the coefficients of the cross-product terms.

Higher-order polynomial models are more accurate but prone to overfitting. To mitigate this, regularization adds a penalty term to balance model weights. Finding the right balance between polynomial order and regularization is crucial for model generalization, which is the ability to perform well on unseen data. We assess generalization through cross-validation, selecting optimal hyperparameters via grid search to maximize model performance for each function $h_i$.

First, we define the complete set of possible hyperparameters combinations for the surrogate model, focusing on two primary factors: the polynomial order and the penalization weight.

**Polynomial order:** We consider polynomial orders ranging from 1 to 4:

$Polynomial\ Order \in \{1, 2, 3, 4\}$

**Penalization Weight:** The penalization weight $\lambda$ is evaluated over the following set of values:

$\lambda \in \{0.01, 0.013, 0.016, 0.02, 0.025, 0.032, 0.04, 0.05, 0.063, 0.079, 0.1, 0.126, 0.158, 0.2, 0.251,$
$0.316, 0.398, 0.501, 0.631, 0.794, 1\}$

We systematically explore all combinations of these hyperparameters using a grid search methodology to select the best configuration for each polynomial model corresponding to the 37 QoIs.
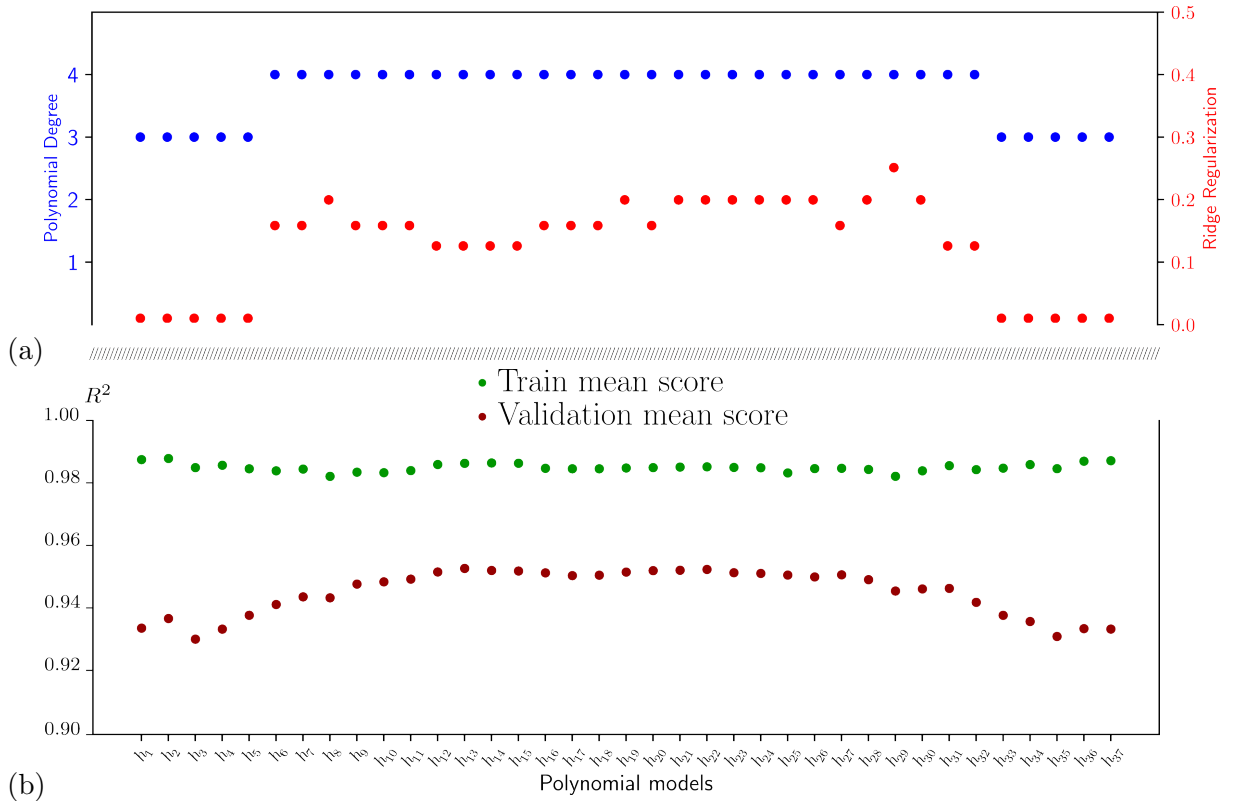


**Figure 6**: Polynomial model hyperparameters and cross-validation results: (a) selected hyperparameters that maximize cross-validation scoring (b) cross-validation means results over the training/testing k-fold cross validation loop

Figure 6a shows the hyperparameters resulting from the search grid methodology, and each predictive model for each QoI results in different hyperparameters. As shown in Figure 6b, the polynomial models capture at least more than 92% of the variance within the data.

## 2.4   THERMAL MODELING PARAMETER ESTIMATION

The estimation of the modeling parameters that best match the experimental observations is achieved with an optimization method. The optimization problem is formulated with the following equation:

$$\boldsymbol{\theta}_{\text{opt}} = \arg\min_{\boldsymbol{\theta}} \mathcal{J}(\boldsymbol{\theta}) \tag{10}$$

with the cost function $\mathcal{J}(\boldsymbol{\theta})$ define the dissimilarity between the surrogate model-predicted numerical weld pool and the experimental weld pool. As the weld pool geometries are described with 37 rays that are similar in length for the experimental weld pool and the numerical weld pool, the dissimilarity between the numerical weld pool and the experimental weld pool is calculated as the mean square error difference. The cost function is defined as the mean square error difference between the predicted numerical weld pools as follows:

$$\mathcal{J} \quad : \quad \mathbb{R}^5 \quad \rightarrow \quad \mathbb{R}$$

$$\boldsymbol{\theta} = \begin{bmatrix} a_f \\ \alpha \\ \beta \\ \eta \\ cc \end{bmatrix} \quad \mapsto \quad \mathcal{J}(\boldsymbol{\theta}) = MSE\left( \begin{bmatrix} h_1(\theta) \\ h_2(\theta) \\ \vdots \\ h_{37}(\theta) \end{bmatrix}, \begin{bmatrix} r_1 \\ r_2 \\ \vdots \\ r_{37} \end{bmatrix} \right) = \frac{1}{37}\sum_{i=1}^{37}(h_i(\theta) - r_i)^2$$

The minimization of the cost function is done via an optimization algorithm, namely quasi-Newton algorithm. The optimization algorithm illustrated in the figure summarizes the workflow. The optimization algorithm works iteratively and the initial guess $\boldsymbol{\theta}_0$ is used as an initialization of the optimization loop. Iterations after iterations, a new guess is proposed that increasingly minimizes the cost function; when no further optimization of the cost function is possible, the optimum set of parameters $\boldsymbol{\theta}_{opt}$ is reached.
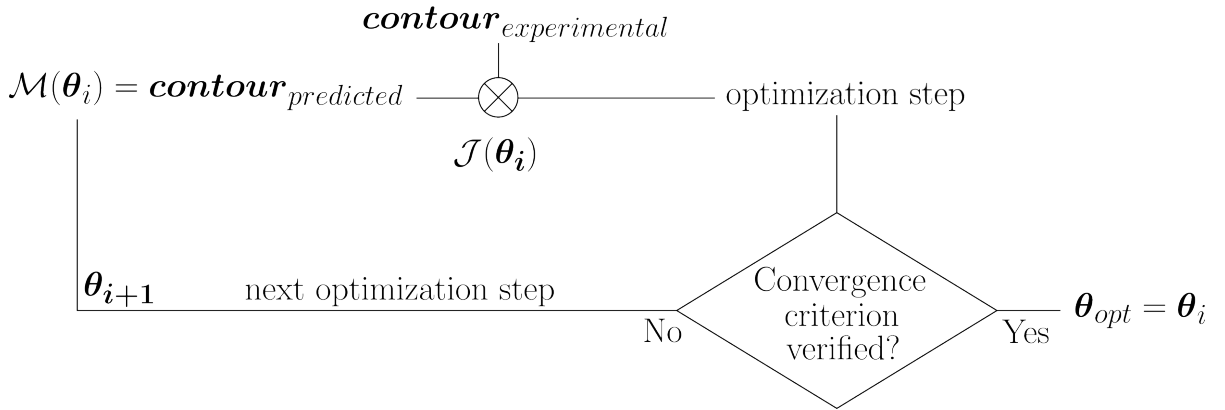


**Figure 7**: Representative diagram for the optimization of the modeling weld pool to the experimental weld pool

## 3   RESULTS AND DISCUSSION

To test the robustness of this methodology, we used synthetic data generated by a reference finite element analysis (FEA). The weld pool contour from this reference FEA was used as input in the optimization loop, replacing the experimental data. The goal was to assess whether the method could accurately identify the parameters $\boldsymbol{\theta}_{ref}$ used in the reference FEA.

The parameters $\boldsymbol{\theta}_{ref}$ were randomly selected within the range of variation of unknown parameters defined in Equation 6. This reference weld pool contour was then used as input for the inverse problem. The optimization process aims to produce an optimal parameter set $\boldsymbol{\theta}_{opt}$, which should closely match $\boldsymbol{\theta}_{ref}$. Finally, a new FEA was conducted using $\boldsymbol{\theta}_{opt}$, and the resulting weld pool contour was compared to that obtained during the optimization loop with the surrogate model.

|  | $a_f(mm)$ | $\alpha$ | $\beta$ | $\eta$ | $cc$ | MSE |
|---|---|---|---|---|---|---|
| $\boldsymbol{\theta}_{ref_1}$ | 2.82 | 3.54 | 1.32 | 0.64 | 2.38 | - |
| $\boldsymbol{\theta}_{opt_1}$ | 2.64 | 4.13 | 1.46 | 0.66 | 5.0 | 5.8e-4 |
| $\boldsymbol{\theta}_{ref_2}$ | 3.69 | 3.90 | 1.24 | 0.65 | 2.93 | - |
| $\boldsymbol{\theta}_{opt_2}$ | 3.21 | 4.45 | 1.35 | 0.65 | 2.95 | 6.5e-2 |
| $\boldsymbol{\theta}_{ref_3}$ | 4.55 | 4.43 | 0.56 | 0.75 | 4.03 | - |
| $\boldsymbol{\theta}_{opt_3}$ | 4.18 | 4.85 | 0.54 | 0.75 | 4.38 | 4.9e-3 |

**Table 3**: Reference and optimized parameters for the inverse problem with corresponding MSE.

Table 3 presents the results of the inverse problem optimization using synthetic data. The reference parameter sets ($\boldsymbol{\theta}_{ref}$) and the corresponding optimized parameter sets ($\boldsymbol{\theta}_{opt}$) are shown along with the mean squared error (MSE) between the reference and optimized weld pool contours. The low MSE values for all three cases indicate that the optimization process was successful in identifying parameter sets that closely reproduce the reference weld pool contours.
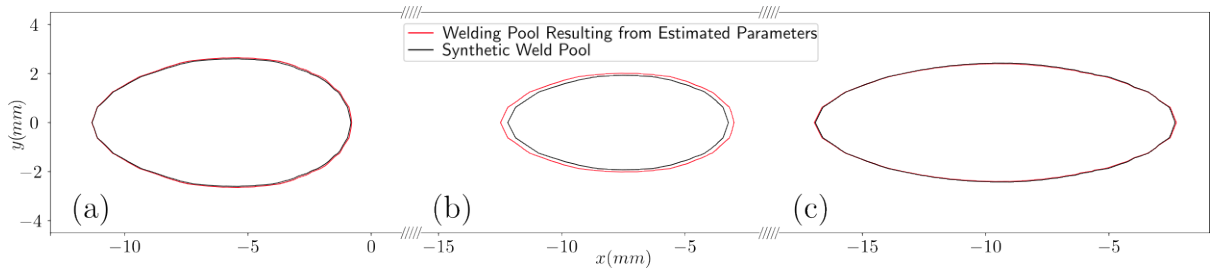


**Figure 8**: Comparison of synthetic (or reference) weld pools (black lines) and weld pools resulting from FEA conducted after parameter estimation (red lines) for three different sets of parameters $\boldsymbol{\theta}$

As shown in Figure 8, the three test cases exhibit good agreement between the synthetic weld pool and the numerical weld pool resulting from the estimated parameters. The optimization method with the surrogate model is able to estimate an optimal set of parameters $\boldsymbol{\theta}_{opt}$ that find the right weld pool contour used as input in the inverse problem. Thus, the optimization approach is used for parameter estimation on the experimental configuration described in section 2 (page 3).

|  | $a_f(mm)$ | $\alpha$ | $\beta$ | $\eta$ | $cc$ | MSE |
|---|---|---|---|---|---|---|
| $\boldsymbol{\theta}_{opt_1}$ | 2.61 | 4.1 | 2.0 | 0.8 | 1.0 | 0.65 |
| $\boldsymbol{\theta}_{opt_2}$ | 4.54 | 2.38 | 0.96 | 0.8 | 1.0 | 1.12 |

**Table 4**: Inverse problem optimal sets of parameters $\boldsymbol{\theta}_{opt_1}$ and $\boldsymbol{\theta}_{opt_2}$

Let's note that the surrogate model is used as a substitute of the FEA within the optimization loop. This allows reducing significantly the computational time and memory resources. The surrogate model allows predicting the QoI in approximately 3 $ms$ against 13 $min$ with the FEA. Thanks to this short computation time, 30 optimization loops are ran with different initialization parameters $\boldsymbol{\theta}_0$. From these 30 tests, two optima are reached as presented in Table 4. These two optima are the solutions of the inverse problem with the experimental weld pool contour observed for the GTAW operation presented in section 2. These two solutions suggest that the optimal equivalent heat source distribution function can either be highly concentrated at the longitudinal front part (with $a_f = 2.61$ $mm$) or exhibit a broader distribution with a larger frontal radius ($a_f = 4.54$ $mm$). The rear radius ($a_r = \alpha \times a_f$) is found to be more spread out in both solutions ($a_{r_1} = 10.7$ $mm$ and $a_{r_2} = 10.8$ $mm$). For the transverse radius ($b = \beta \times a_f$), both solutions have similar values ($b_1 = 5.22$ $mm$ and $b_2 = 4.35$ $mm$).

These results lead to two possible physical interpretations. Both interpretations share a conductivity coefficient multiplier equal to 1 ($cc = 1$), suggesting that heat convection within the melt pool is not significantly involved in this welding scenario. Additionally, the spread of heat towards the rear in both cases indicates that the heat input by the arc is distributed more in the opposite direction of welding. The primary difference lies in the front distribution, where the heat input by the arc could either be very concentrated at the front or more spread out.
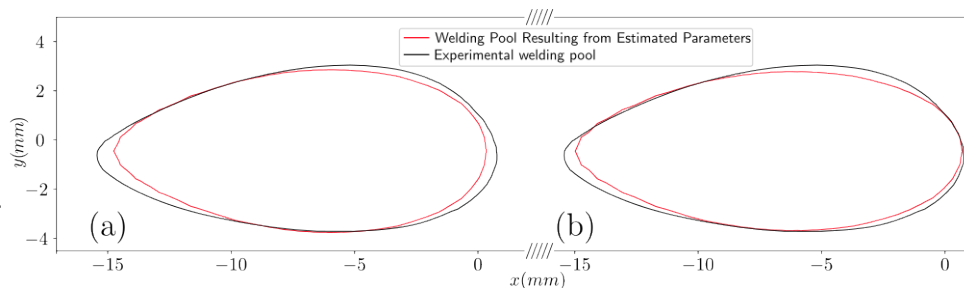


**Figure 9**: Parameter estimation from an experimental weld pool contour. Comparison between experimental contour and numerical weld pool contour: (a) first solution (b) second solution.

These two solutions give similar weld pool contour that match quite well the experimental weld contour as shown in Figure 9. This suggests that the defined inverse problem is ill-posed according to Hadamard's definition. This issue of inverse problems is well documented in the literature. To address the ill-posed nature of the problem, consider regularization or Bayesian inference.

This work was based on the weld pool contour measured in thermal steady state. It could be possible to enhance the input data used in the inverse problem by mixing measurements: weld pool contour and some local temperatures away from the weld pool. Perhaps, the use of weld pool contour at the ignition of the arc until it reaches the thermal steady state could give

relevant data and leads to an unique solution of the inverse problem.

## 4 CONCLUSIONS

In this work, a methodology was proposed for heat source parameter estimation. A surrogate model has been trained and used to replace the FE analysis in the optimization loop. The experimental data required, in the optimization loop, is the weld pool contour (solid - liquid interface). A camera was used to record the weld pool as it is a non-intrusive and non-destructive technique. The surrogate model established maps the heat source parameters to the weld pool contour. By using a machine learning methods to construct the surrogate model, the estimation of the modeling parameters can be achieved within few seconds.

## REFERENCES

[1] Sindo Kou. "Residual Stresses, Distortion, and Fatigue". In: Welding Metallurgy. John Wiley Sons, Ltd, 2002. Chap. 5, pp.122–141. isbn: 9780471434023. doi:10.1002/0471434027.ch5.

[2] Q. Wu, T. Mukherjee, A. De, T. DebRoy. "Residual stresses in wire-arc additive manufacturing – Hierarchy of influential variables". In: Additive Manufacturing 35 (2020).

[3] Stephen Cadiou. "Modélisation magnéto-thermohydraulique de procédés de fabrication additive arc-fil (WAAM)". Thesis. Université de Bretagne Sud, Dec. 2019. url: https://theses.hal.science/tel-02496906.

[4] John Goldak, Aditya Chakravarti, and Malcolm Bibby. "A new finite element model for welding heat sources". In: Metallurgical Transactions B 15 (June 1984), pp. 299–305.

[5] Junquiang Wang , Jianmin Han, Joseph Domblesky, Zhiyong Yang, Yingxin Zhao, Qiang Zhang. "Development of a new combined heat source model for welding based on a polynomial curve fit of the experimental fusion line". In: The International Journal of Advanced Manufacturing Technology 87 (Nov. 2016).

[6] Jianfeng Yue, Hao Zhou, Chang Xie, Wei Zhou, Wenji Liu. "Temperature field simulation and asymmetric heat transfer distribution of dissimilar steel welded with external transverse magnetic field". In: Materials Today Communications 37 (2023), pp. 107-141.

[7] Masahiro Kusano, Houichi Kitano, and Makoto Watanabe. "Novel Calibration Strategy for Validation of Finite Element Thermal Analysis of Selective Laser Melting Process Using Bayesian Optimization". In: Materials, 14(17) (2021).

[8] Sami Hilal. "Thermo-mechanical modelling of the Wire Arc Additive Manufacturing process (WAAM)". Thesis. Université Paris sciences et lettres, May 2022. url: https://pastel.hal.science/tel-03868998.

[9] Navid Moslemi, Soheil Gohari, Behzad Abdi, Izman Sudin, Hamidreza Ghandvar, Norizah Redzuan, Shukur Hassan, Amran Ayob, Sehun Rhee. "A novel systematic numerical approach on determination of heat source parametersin welding process". In:Journal of Materials Research and Technology 18 (2022), pp. 4427–4444.